

***Final Draft***  
**of the original manuscript:**

Abibe, A.B.; Sonogo, M.; dos Santos, J.F.; Canto, L.B.; Amancio-Filho, S.T.:  
**On the feasibility of a friction-based staking joining method for  
polymer–metal hybrid structures**  
In: Materials and Design (2015) Elsevier

DOI: [10.1016/j.matdes.2015.12.087](https://doi.org/10.1016/j.matdes.2015.12.087)

**On the feasibility of a friction-based staking joining method for polymer-metal hybrid structures**

A.B. Abibe <sup>a, b</sup> – andre.abibe@hzg.de

M. Sônego <sup>a, b, c</sup> – mrl.sonego@gmail.com

J.F. dos Santos <sup>a</sup> – jorge.dos.santos@hzg.de

L. B. Canto <sup>c</sup> – leonardo@ufscar.br

S.T. Amancio-Filho <sup>a, b, \*</sup> - sergio.amancio@hzg.de

<sup>a</sup> Helmholtz-Zentrum Geesthacht, Institute of Materials, Materials Mechanics, Solid State Joining Processes (WMP) – Max Planck Strasse 1, D-21502 Geesthacht, Germany

<sup>b</sup> Helmholtz-Zentrum Geesthacht, Institute of Materials Research, Materials Mechanics, Advanced Polymer-Metal Hybrid Structures Group – Max Planck Strasse 1, D-21502 Geesthacht, Germany

<sup>c</sup> Federal University of São Carlos (UFSCar), Department of Materials Engineering (DEMa) – Rod. Washington Luiz km 235, CEP 13565-905, São Carlos-SP, Brazil.

\*Corresponding author:

Sergio de Traglia Amancio-Filho

Max-Planck Strasse 1, D-21502 Geesthacht, Germany

Tel: +49 4152 87 2066

Fax: +49 4152 87 2033

sergio.amancio@hzg.de

## HIGHLIGHTS

- A friction-based alternative (F-ICJ) to current staking joining methods is presented
- The new method is feasible with transportation industry materials (PEI/AA6082-T6)
- Sound joints can be produced in short cycles (3-20 seconds)
- Effects of heat input on joint microstructure and local properties are elucidated
- The mechanical performance and failure mechanisms of F-ICJ joints are described

## ABSTRACT

The increased use of hybrid structures to reduce weight and the limitations of the traditional technologies create a niche for new joining techniques. Injection Clinching Joining (ICJ) was recently introduced as a new joining technique based on staking, injection molding and mechanical fastening.

This technique consists of using an energy source to soften/melt a protruding stud that is integrated in the polymeric partner and injecting it into the cavity of a metallic, ceramic or polymer-based partner to create a spot joint. The first studies used the principles of ICJ with electric resistance as a heating source; this variant is known as Electrical heating ICJ (E-ICJ). E-ICJ could achieve good mechanical properties but had long cycles because of the convectional energy supply. This paper presents a feasibility study of the new Friction-based ICJ technique (F-ICJ) to investigate alternative energy sources for a faster and more efficient process. The microstructure and mechanical properties of the joints of polyetherimide and aluminum alloy 6082-T6 are discussed and related to temperature development during processing. The effect of tool geometry on the generated shear layer is explained based on rheology theories. Three different microstructural zones are developed in the polymer partner during processing: a thermomechanically affect zone, a heat affected zone, and the base material. The ultimate tensile load of the joint in single lap shear tests ranged from  $712 \pm 34$  N to  $1250 \pm 98$  N. The strength of the stake head was evaluated using cross tensile testing and ranged from  $311 \pm 20$  N to  $585 \pm 10$  N. The primary observed failure modes for F-ICJ joints are presented and briefly described. This preliminary study indicates that the F-ICJ process can produce sound punctual joints in short cycles (3-20 seconds) with potential for improvement in further development.

**KEYWORDS:** staking, polymer-metal structures, hybrid joining, friction joining, polyetherimide

## INTRODUCTION

There is an increasing trend to reduce vehicle weight in the transportation industry because of environmental issues, such as the requirement to reduce CO<sub>2</sub> emissions (Cuenot, 2009), and economic concerns, such as the trend of rising fuel prices (Duflou et al., 2009). The most common strategy for weight reduction is the use of advanced lightweight materials such as polymer composites, engineering thermoplastics and lightweight alloys (Amancio and dos Santos, 2009). This broader selection of materials leads to the use of hybrid structures, where the dissimilarity among materials creates a design and assembly challenge for engineers.

The traditional techniques to join polymeric and metallic parts are mechanical fastening and adhesive bonding. The use of adhesives promotes a continuous contact between the surface of the parts, which results in structures with uniform stress distribution and good mechanical performance under tension, compression and shear (Adderley, 1988). However, the need for extensive surface treatments adds costs and is time consuming. Moreover, solvent evaporation, which is usually found in thermosetting adhesive systems, may result in health and safety hazards (Barnes and Pashby, 2000). Mechanical fastening is largely used because of its simplicity and ease to disassemble. The main limitation is the hole, which acts as a stress concentrator (Amancio and dos Santos, 2009) and allows for earlier crack nucleation, which may result in premature failure. The difficulty in joining

dissimilar materials and the limitations of the traditional techniques to join complex geometries create a niche for new joining techniques (Messler Jr, 1995).

Staking techniques have been studied as an alternative to join hybrid structures by several authors. Hahn and Finkeldey (2003) studied ultrasonic staking and hot-air staking for glass fiber reinforced polyamide; Yeh et al. (1998) used hot-air staking to join various combinations of engineering thermoplastics; Beute (2009) introduced a more efficient and fast concept for infrared staking; DeSouza (2009) used design of experiments to create an optimized design guideline for heat staking at a company. Staking methods are based on the deformation of a protruding polymeric stud, whose diameter fits into a metallic through-hole. This stud is subsequently formed into an anchoring element, which is designated as a stake and is responsible for the mechanical anchoring of the joint. This forming step can be performed at room temperature using sheer pressure, which is known as cold staking (Rotheiser, 1999). Cold forming requires high joining forces and is more efficient with ductile polymers, which do not break during forming. Staking can also be performed using several different energy sources to soften or melt the stud prior to forming. The common energy sources are hot air (Yeh et al., 1998), ultrasonic (Hahn and Finkeldey, 2003), and infrared radiation (Beute, 2009). The “hot staking” methods generate less residual stresses (Rotheiser, 1999) and are applicable to almost any thermoplastic. The main applications of staked joints are in secondary and tertiary structures of automotive industry, electronic devices, and household items. State-of-the-art staking is a simple and low-cost technique, whose main

limitations are the poor surface finishing, and the residual stresses and recovery effects in the case of cold staking (Rotheiser, 1999).

A recent development in staking technologies is the “Injection Clinching Joining” (ICJ) (Amancio-Filho et al., 2010) based on the principles of staking, injection molding, and mechanical fastening. ICJ consists of softening/melting a protruding stud that is integrated in the polymeric partner and injecting it into the cavity of a metallic, ceramic or polymer-based partner to create a spot joint with improved mechanical anchoring performance. The geometries of the components and some joint characteristics of ICJ and staking are similar; however, although the mechanical performance of staking is based on the formation of a protuberant stake head, in ICJ, the filling of the metallic cavities with polymer, which leads to flatter stake heads, is responsible for the mechanical strength of the joint. Therefore, ICJ flat-head joints have better visual aspect and can withstand loading because of the anchoring in the metallic cavities. The application range of ICJ is aimed at the high-end of staking technologies for secondary and tertiary load-bearing structures.

A laboratory prototype for the ICJ process was developed in 2010 (Amancio-Filho et al., 2010). The system uses a hot case, which is heated by electricity as the energy source to soften/melt the stud, and a punch-piston coaxial to the hot case to form the stud into a stake. This technique was called Electrical-heating Injection Clinching Joining (E-ICJ) (Abibe et al., 2011). A typical microstructure of E-ICJ joints of aluminum 2024-T351 and 30% short-fiber reinforced polyamide 66 is shown in Figure 1a. The complete filling of the metallic cavities (chamfer and screw) with the polymer considerably improves the mechanical performance of the joint (Abibe et al., 2013). Figure 1b is a

microtomography of the polymeric partner, which shows a good filling of the metallic cavities by the polymeric partner. This joint was produced in 3 minutes at 300 °C (Abibe et al., 2011). E-ICJ joints with such geometrical characteristics achieved good mechanical performance, where the bearing stress was up to 88% of the tensile stress of the base material (Abibe et al., 2013).

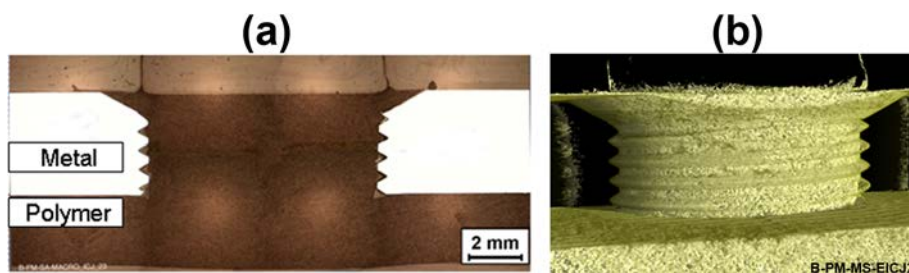


**Figure 1:** Electrical-heating Injection Clinching Joining (E-ICJ): (a) Cross-sectional view of a joint (Adapted from Abibe et al. (2011) with permission); (b) Microtomography of a joint, which shows the polymeric partner. This joint was produced in 3 minutes at 300 °C.

The main advantages of E-ICJ over traditional techniques are the absence of surface preparation, requirement of simple equipment, good mechanical performance, and costs and weight savings by not using extra parts (Abibe et al., 2011). The main limitations of E-ICJ are that it produces only punctual, permanent joints, it is not feasible for thermosets, and it has long joining cycles and low energy efficiency because of the heat transfer by convection (Abibe et al., 2011).

Considering the limitations of current staking and E-ICJ, a niche for a high-end staking technology was identified. To achieve high energy efficiency with fast cycles and good mechanical performance, a friction-based variant of

ICJ is proposed. The energy efficiency of frictional processes is shown in analytical (Neumann and Schober, 1991; Schaefer, 1971) and numerical (Chao et al., 2003) models for heat transfer in friction welding, which report more than 95% energy efficiency for the process. Additionally, the principles of ICJ contribute to improved mechanical performance (Abibe et al., 2013).

This paper describes the principles of the Friction-based Injection Clinching Joining (F-ICJ) process, and the feasibility of joints between AA6082-T6 aluminum alloy and polyetherimide (PEI) is demonstrated. The F-ICJ joints are analyzed in terms of thermal history, microstructure, local and global mechanical properties. The failure modes that are observed in lap-shear and cross-tensile tests are described.

## MATERIALS AND METHODS

The polyetherimide (PEI) that was used is a commercial-grade Duratron PEI U1000, which was supplied by Quadrant Plastics (Lenzburg, Switzerland). It is an amorphous thermoplastic with high mechanical strength and stiffness. It exhibits excellent thermal stability with glass transition temperature ranging from 215 to 220 °C and decomposition occurring above 490 °C (Amancio-Filho et al., 2008). The main applications of PEI are in the aircraft, medical, packaging, and automotive industry (Carrocio et al., 2012).

The metallic partner is the 6082-T6 aluminum alloy. This material is a precipitation hardenable alloy, whose main alloying elements are magnesium

(0.6-1.2%) and silicon (0.7-1.3%) (Aalco, 2011). AA6082-T6 is a medium-strength aluminum alloy with excellent corrosion resistance, good formability, weldability and machinability. It is typically used in highly stressed structures such as trusses, bridges, cranes, and transportation applications (Aalco, 2011).

The specimens were machined from 6.25-mm-thick extruded PEI plaques and 2-mm-thick rolled AA 6082-T6 plates. The polymeric part had a 4 mm height and 6 mm diameter stud that protruded from its surface, which was fitted into the machined through-hole on the metallic part. A surface radius of 0.3 mm was used at the base of the stud. The metallic part had a chamfer cavity design (Figure 2a). The geometries are described in Figure 2.

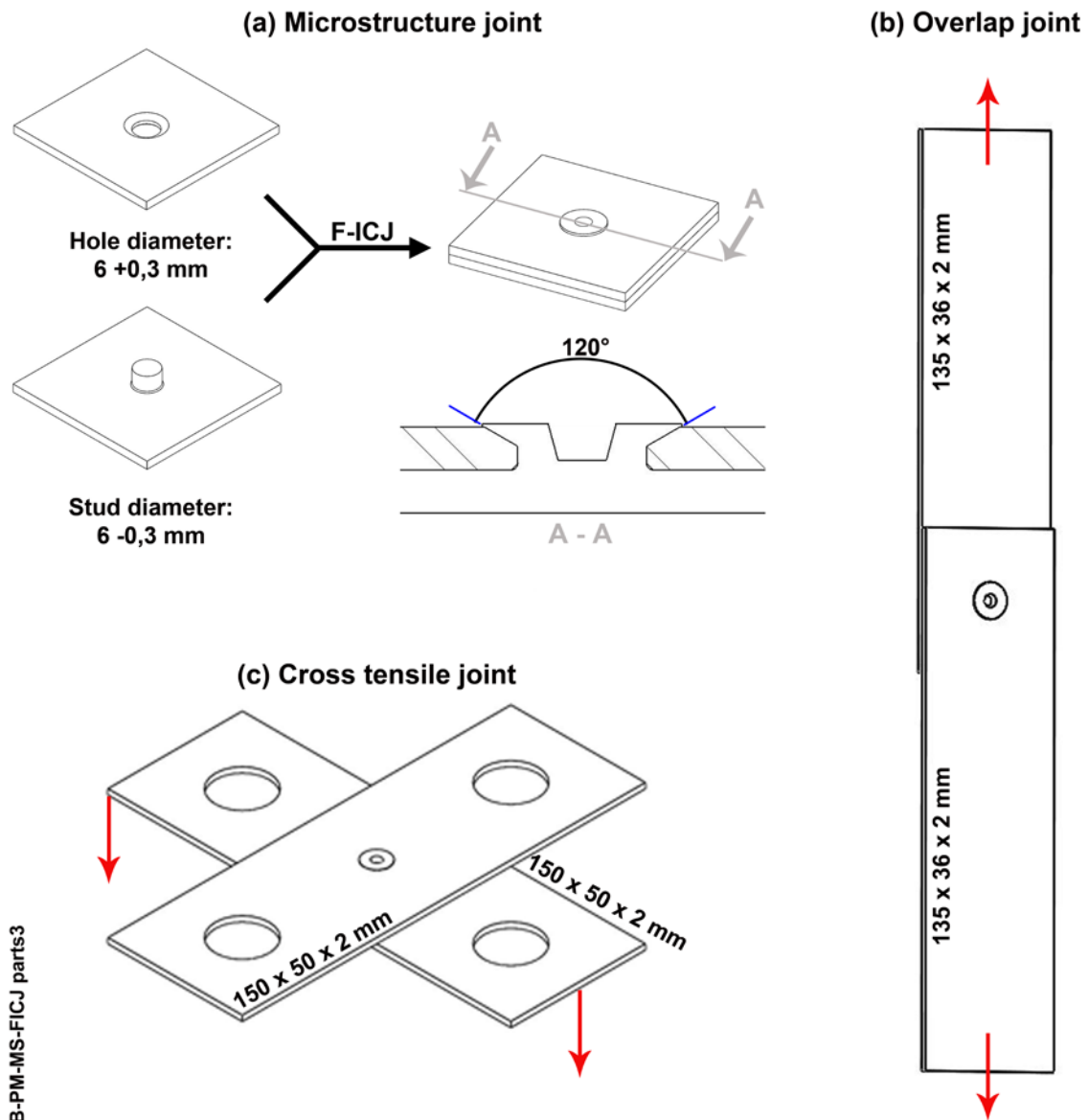


**Figure 2: Configuration of F-ICJ joints: (a) joint for microstructural analyses and local mechanical properties testing; (b) overlap specimen for the lap shear strength test and (c) cross tensile specimen to evaluate the stake head strength.**

The F-ICJ joints were produced using a cylindrical, non-consumable tool that was coupled with a high-rotational-speed friction welding machine (RSM 400, Harms & Wende, Hamburg, Germany). The tool was machined from AISI

316L stainless steel bars. The frictional torque was measured with a torque-measuring system (Kistler Instrumente AG, Winterthur, Switzerland), which was mounted on a backing plate. The AA 6082-T6/PEI joints were obtained within the following processing window: rotational speed of 8000-15000 rpm, frictional pressure of 0.2-0.8 MPa, frictional time of 2500-5000 ms, forging pressure of 0.6-1.0 MPa, forging time of 2500-5000 ms and holding time of 7.5-10 s. The process parameters were monitored using the RQ-Fuzzy software, which was integrated with the RSM 400 system. An infrared thermo-camera (ImageIR8800, InfraTec GmbH, Dresden, Germany) was used to monitor the thermal history during joining and cooling time.

Two tool designs were used to investigate the effects of tool geometry on the properties and microstructure of F-ICJ joints. The tool designs are schematically shown in Figure 3. To heat a sufficient volume of the stud and efficiently deform it, a pin-tool design was chosen. Compared to a flat-tool design, the pin tool can better distribute the generated heat in the stud volume while maintaining short cycles; in addition, it helps pushing the material outwards to improve the cavity filling of the ICJ joints.

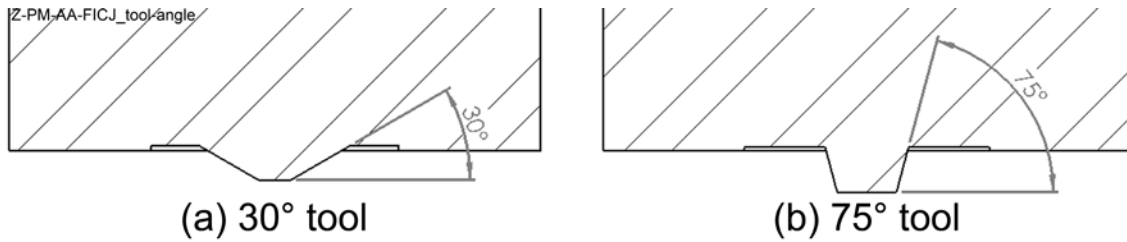


**Figure 3: Tool geometry designs that were named (a) 30° pin tool or (b) 75° pin tool according to the angle between the wall of the pin and its bottom surface (cone angle).**

The microstructure and local mechanical properties were investigated in the joints as shown in Figure 2a. Samples were cut 1 mm from its center, mounted in epoxy resin, ground and polished. Microstructural analysis was performed using stereo and light optical microscopy. Microhardness profiles were used to observe the local changes in mechanical properties. The testing procedure was performed according to ASTM E384 (ASTM, 2010c) using an indentation load of 0.495 N and a holding time of 15 s with a Zwick ZHV (Zwick GmbH & Co. KG, Ulm, Germany) microhardness tester.

The global mechanical properties of the joints were evaluated through single lap shear tests on overlap joint specimens (Figure 2b) using a Zwick 1478 (Zwick GmbH & Co. KG, Ulm, Germany) universal testing machine at room temperature and a crosshead speed of 2 mm/min; the test procedure was based on ASTM D5961 (ASTM, 2010b). The clamps were aligned to the longitudinal axis of the specimen. A digital image correlation system (DIC) – Aramis (GOM mbH, Braunschweig, Germany) – was used to monitor the sample strain distribution during the tests.

The mechanical strength of the stake head was evaluated through cross tensile testing (Figure 2c) using a Zwick 1478 (Zwick GmbH & Co. KG, Ulm, Germany) universal testing machine at room temperature and a crosshead speed of 2 mm/min; the test procedure was based on DIN ISO 14272 (DIN, 2002). In this configuration, the top metallic plate was fixed, whereas the lower polymeric plate was pulled away.

## PRINCIPLES OF FRICTION-BASED INJECTION CLINCHING JOINING (F-ICJ)

F-ICJ is a new approach to the ICJ technique ([patent application](#)) (Abibe et al., 2011) to join hybrid structures of thermoplastics and metals. ICJ processes produce joints by heating and deforming a polymeric stud that is inserted into a through-hole (metallic cavity) to create a stake that mechanically anchors the joining partners (Amancio-Filho et al., 2010). Although E-ICJ uses electrical heating, F-ICJ is based on frictional heating, which is faster and more energy-efficient.

A schematic drawing of the F-ICJ process is shown in Figure 4. In Figure 4a, the parts are aligned with the tool, and the thermoplastic stud is inserted into the cavity of the metallic partner. The rotating tool approaches the stud (Figure 4b) and touches it to generate frictional heat (friction step - Figure 4c). This friction step creates the first softened/melted polymer volumes and is followed by the deceleration of the rotational speed until stopping, whereas the axial pressure is increased to push the softened volumes to the cavities and give the stake head the final form (forging step - Figure 4d). After a short cooling time

under pressure (Figure 4e), the tool retracts, and the staked joint is formed (Figure 4f).

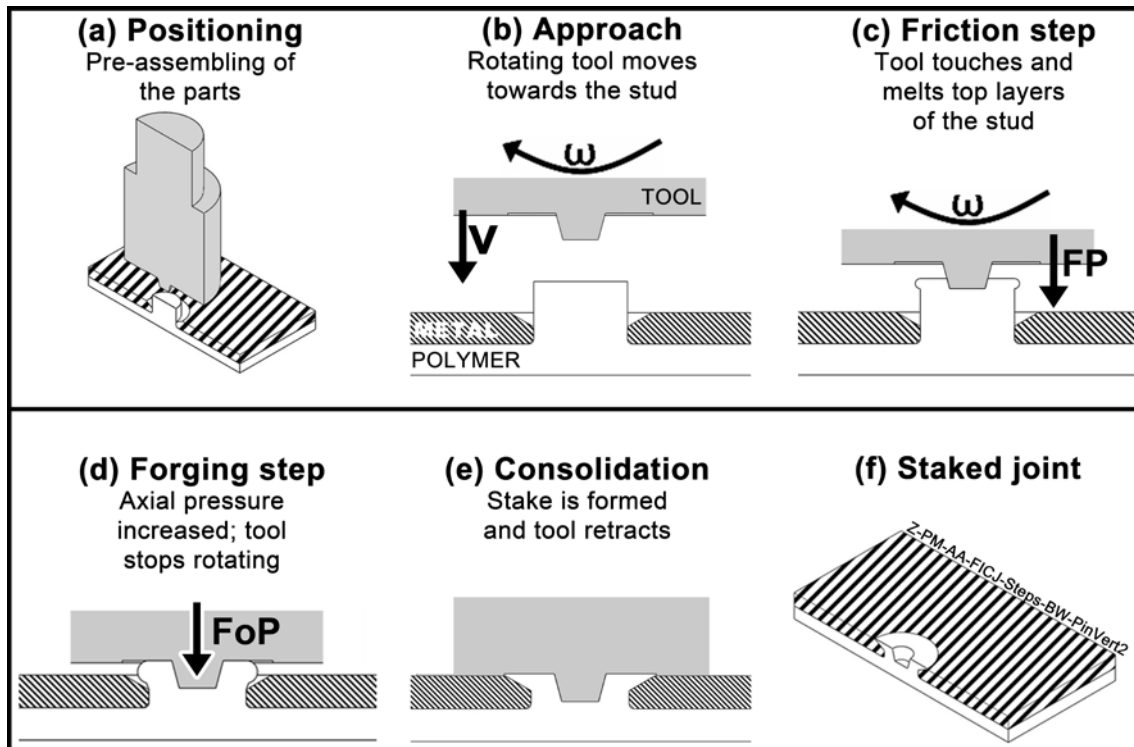


**Figure 4: Stages of the F-ICJ process using a pin tool: (a) Positioning of the polymeric stud into the metallic cavity; (b) approach of the rotating tool; (c) friction step when polymer is softened/melted; (d) forging step when rotational speed is decreased and an increased axial pressure is applied by the tool; (e) consolidation of the polymer under pressure in the metallic cavity; (f) staked joint.**

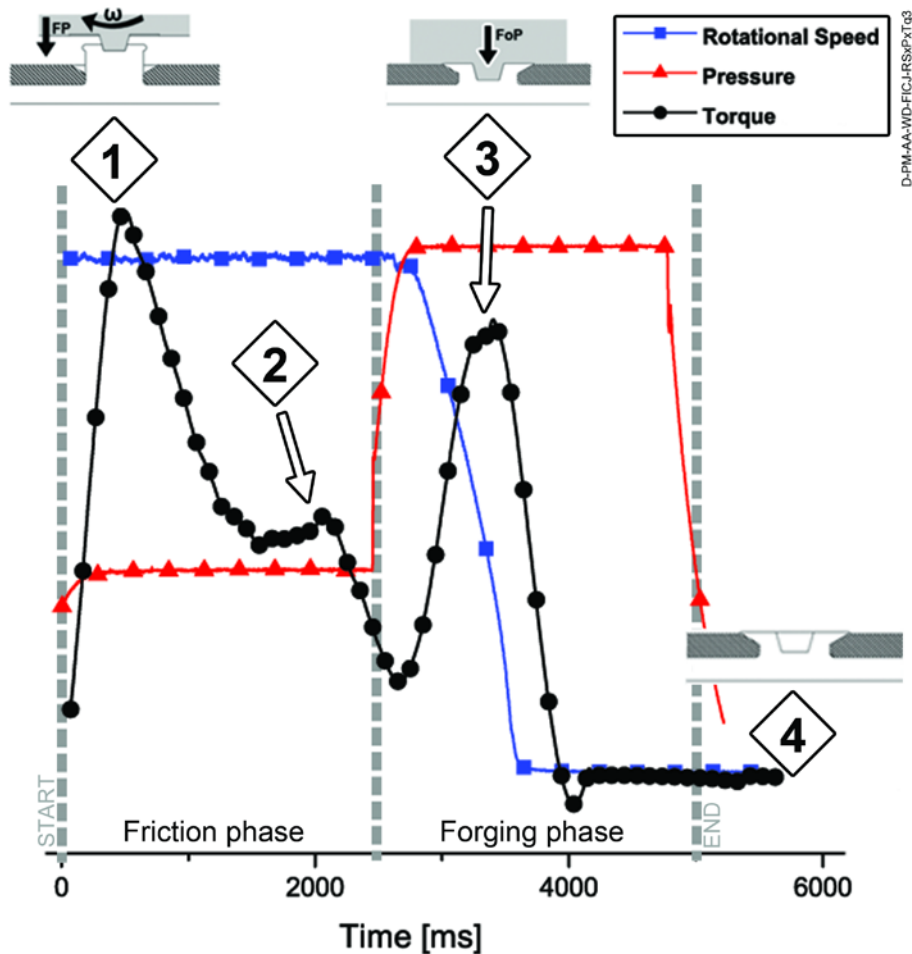
In this process, it is possible to use different tool designs and create different stake geometries. For example, a pin tool produces a hollow stake, whereas a flat tool creates a solid stake with a flat surface. The tool design

should be chosen according to the thermal and rheological properties of the polymer, the geometries of the joining partners, and their hole clearances.

The metallic through-hole is designed with cavities such as threads and/or a chamfer to improve the mechanical interlocking of the polymer and increase the contact surface of the stake with the metallic partner. In an optimized process, the polymeric stud volume efficiently fills these cavities and increases the mechanical anchoring, which results in an improved global mechanical performance.

### **Process phases**

The F-ICJ process can be divided into two main phases: the friction phase, which is characterized by high rotational speed and low axial pressure, and the forging phase with high axial pressure and decreased rotational speed. Figure 5 explains the F-ICJ phases based on the monitoring curves from the RQ Fuzzy software and the torque-measuring sensor.



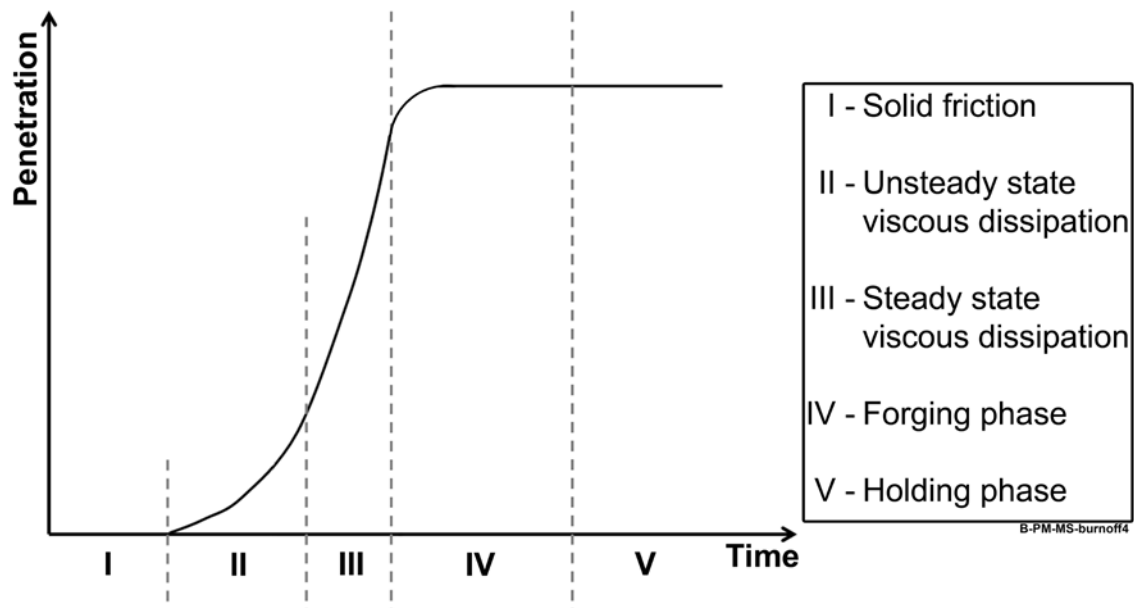
**Figure 5: Phases of the F-ICJ process related to the monitoring curves of rotational speed, pressure, and torque. The steps 1 to 4 are related to phenomena occurring in the process.**

Figure 5 shows the typical curves of rotational speed (blue squares), pressure (red triangles) and torque (black circles) of an F-ICJ joining cycle. During the friction stage, the solid-solid contact of the rotating tool with the thermoplastic stud generates frictional heat and produces a torque peak (stage 1). The torque decreases when the stud is softened by the generated frictional heat. At stage 2, an intermediary peak in the torque curve appears. Such peaks during the friction phase result from the recurring contact with solid and

softened/melted material because of the squeeze flow of the softened/melted volumes into the cavities and the surroundings. In the forging phase, the rotational speed decreases to zero. In this stage, there is a torque peak because of the decreased heat input and increased axial pressure (stage 3), which implies solid-solid contact. In stage 4, after a short holding time, the tool retracts, and the stake is formed.

### **Heat generation by friction in F-ICJ**

The thermal energy produced by a friction process has two components: an internal friction because of plastic deformation and a surface friction (sliding), whose nature remains unclear (Chen and Li, 2005). The process temperature is a function of the set-up axial pressure and rotational speed, and of the coefficient of friction, density, and thermal conductivity of the materials (Potente, 2004). Similar to most friction welding processes, the F-ICJ process can be divided into five distinctive phases as shown in Figure 6.



**Figure 6: Schematic curve that represents the tool penetration in a friction welding process. Based on Stokes (1988a).**

Phase I is characterized by solid friction. The polymer-tool interface is subjected to a normal pressure, and the contact of the rotating tool with the solid stud induces Coulomb friction, which heats the materials until the polymer is softened/melted. During this notably short phase, the tool axial displacement almost does not change (approximately zero), whereby the temperature increases because of the plastic deformation of the surface microscopic roughness peaks.

Phase II is known as “unsteady state viscous dissipation”. It starts when a softened/melted polymer layer is created at the polymer-tool interface. In this phase, energy is mainly generated by viscous heating in the melted polymer. Thermal energy is released from the breaking of the secondary bonds among the chains because of the tool-shearing action, chain disentanglement and flow

(Billmeyer Jr, 1971). At the beginning, the softened/melted film is thin; therefore, the shear rate is high, which induces a high viscous heating and an intense melting rate at the polymer-tool interface (Stokes, 1988a). In addition, the material flow to the side is small when there is a thin softened/melted polymer layer. However, the thickness of the softened/melted polymer layer increases with time, which reduces the shear rate and the melting rate. Therefore, the squeeze flow is further supported.

Eventually, an equilibrium between the polymer softening/melting at the interface and the squeezed outflow is reached, and the axial displacement increases linearly with time (Stokes, 1988a). The process is steady, and phase III, known as “steady state viscous dissipation”, occurs.

Phase IV is known as the “forging phase” and starts when the axial pressure is increased and the rotational speed of the tool is decreased. The melted polymer continuously flows outwards until its viscosity increases and consolidation is achieved during cooling (Stokes, 1988b). This stage helps eliminating defects such as air bubbles in the softened/melted volume. The last phase (phase V) is called the “holding phase”. In this stage, there is no squeeze flow. The tool stays in contact with the solidifying polymer, which avoids undesired deformation of the stake head during cooling because of shrinkage and recovery effects.

### **Controlling parameters and variables**

The main controlling parameters of F-ICJ are rotational speed (RS), frictional time (FT), frictional pressure (FP), forging pressure (FoP), forging time

(FoT), and holding time (HT). In the friction phase, RS, FT, and FP are active in heat generation. RS is the speed of the tool during the friction phase, which is decelerated at the start of the forging phase, but it contributes to generate frictional heat during the friction phase. FT is the length of time of the friction phase, where the rotational speed is at its set level and generates heat. FP is the axial pressure of the spindle during the friction phase. The frictional pressure keeps the tool in contact with the stud to make it reach solid volumes when the softened/melted layers are squeezed out.

During the forging phase, FoP, FoT, and HT define the final shape of the stake. FoP is the axial pressure of the tool during the forging phase. The forging pressure is higher than the frictional pressure and serves to form the final shape of the stake. FoT is the length of time during which the stake is under the forging pressure; this parameter determines the length of the forging phase and is important to the joint consolidation. Finally, HT is the length of time during which the tool remains in contact with the stake before tool retraction. HT is relevant to reduce the recovery effects and polymer shrinkage.

These parameters are described for a time-controlled process as presented in this work. With adequate equipment, F-ICJ can be performed in force-control or displacement-control modes. For these other variants, the importance and effect of the parameters may vary and require specific investigation for their descriptions.

## **Joint microstructure**

Figure 7 shows a schematic drawing of the microstructural zones that are observed in F-ICJ joints for joining using a pin tool. This tool design generates a hollow stake.

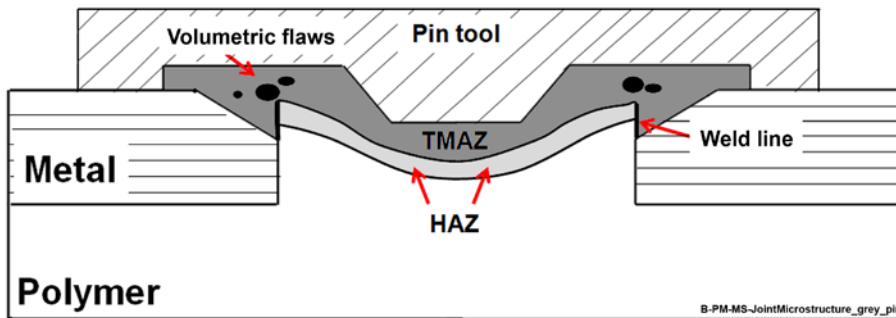


**Figure 7: Microstructural zones of F-ICJ joint with a hollow stake, which is produced using a pin tool.**

Heat and mechanical deformation modify the microstructure and properties of the polymer during the F-ICJ process. A volume of the polymeric stud is softened/melted and deformed by the contact with the rotating tool. Depending on the temperatures and the strain rates, recrystallization, chain reorientation, and thermal degradation can occur in the polymer. Higher temperatures also decrease the viscosity of the material, which makes it easier for air to be entrapped in this volume; thus, some volumetric flaws such as air bubbles can occur.

Furthermore, a certain amount of this volume fills the metallic cavity. In similar friction joining processes, this volume is described as a thermomechanically affected zone (TMAZ) because of the combined action of

mechanical deformation and temperature. Another intermediary microstructural region can appear under the TMAZ, which is affected by heat conducted from the TMAZ, but can also have mild deformation effects because of the hydrostatic pressure that the tool applies over the softened/melted volume. Recovery effects such as microcracking and physical aging can occur in this volume. This zone is traditionally described as the heat affected zone (HAZ), and the polymer temperature at the HAZ during the joining process is usually below glass transition temperature.

The interface between the TMAZ and the HAZ can be noticed with sharp differences in the microstructure such as partial fiber breakage in reinforced polymers (Abibe et al., 2011) and changes in refraction index for transparent polymers (Stokes, 2001). This is a strong polymer-polymer interface. The boundary between the HAZ and the unaffected volume of the base material (BM) is notably difficult to visualize or define because most effects only occur in the macromolecular scale. Microhardness and thermal analyses can also be used to identify changes in the local properties at the stake to define the borders between the microstructural zones. At the top of the stake head, a weld line between the TMAZ and the HAZ/BM can be formed, namely between the squeeze-flowed material over the chamfer and the unaffected stake volume (see Figure 7).

Because the interaction of the tool with the joining partners is limited to the polymer, the achieved temperatures during a typical F-ICJ process are not high enough to cause significant heat transfer to the metal, which can cause microstructural changes. In some cases, the rotating tool lightly touches the metallic partner, which causes a partial dynamic recrystallization in a thin layer

(up to 100  $\mu\text{m}$ ) on the metal surface because of thermomechanical work. However, because this phenomenon occurs in a notably thin layer of the metal and because the polymeric partner is usually where failure occurs during loading, this change is not relevant to the global behavior of F-ICJ joints.

## RESULTS AND DISCUSSION

### **Thermal monitoring of F-ICJ process**

The thermal history throughout the F-ICJ process was recorded using an infrared thermo camera that focused at the rotating tool (Figure 8). The tool surface temperature was monitored during the friction, forging and holding phases (Figure 8a). After the tool retraction, the temperature of the polymer stake head was monitored (Figure 8b). The measurement areas are marked in Figures 8a and 8b. A typical temperature cycle of the tool (blue-square curve) and the polymer stake (red-triangle curve) is shown in Figure 8c with the corresponding stages of the process.

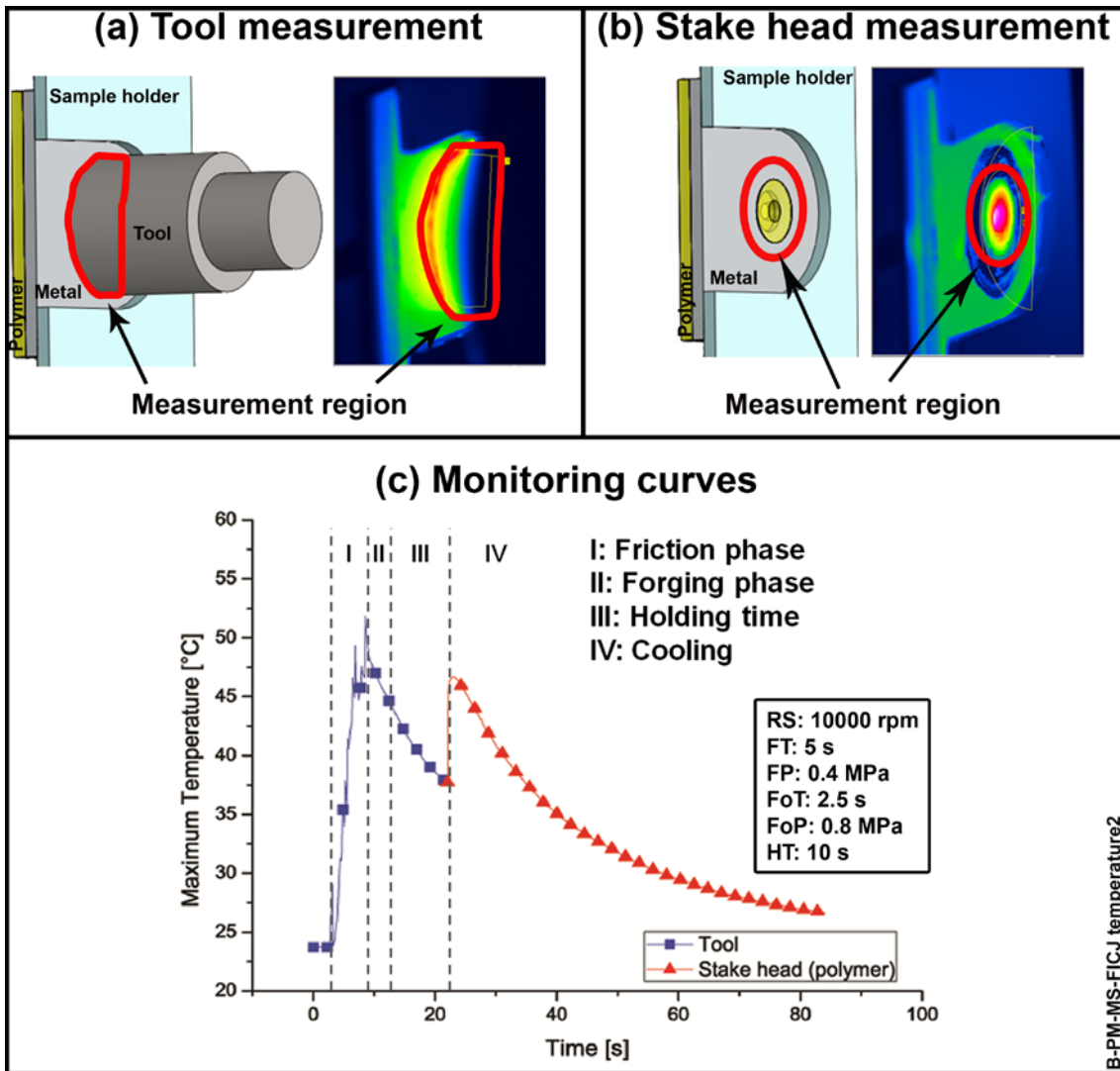


Figure 8: Thermal monitoring of the F-ICJ process for a typical joint: (a) the temperature profile of the tool and the measurement area for the blue-square curve in (c); (b) the temperature profile of the stake head and measurement area for the red-triangle curve in (c); (c) plots of maximum temperature of the tool (blue-square curve), which was achieved in the measurement region in (a), and the maximum temperature of the polymer stake head (red-triangle curve), which was achieved in the measurement region in (b).

The monitoring of the tool temperature qualitatively shows the heat generated during the friction phase. As the interface tool-stud is heated, the surface of the tool warms up and cools down again after the friction phase throughout the forging and holding phases (see Figure 8c). Although the tool temperature can be monitored, the peak temperature at the interface is notably complicated to measure because of the tool movement. A method to estimate this temperature is by analytical modeling or using a complex thermometric remote system that is installed in the tool, which is not the scope of this work. As a more reliable response of the heat input into the process, the peak temperature that was measured at the stake head after the tool retraction was recorded (the temperature peak is circled in Figure 8c).

In the studied parameter range, the average maximum stake head temperature ranged from  $43 \pm 4$  °C (for low-heat-input joints such as RS: 8000 rpm; FT: 2500 ms; FP: 0.3 MPa; FoT: 5000 ms; FoP: 0.7 MPa; HT: 7.5 s) to  $95 \pm 9$  °C (for high-heat-input joints such as RS: 12000 rpm; FT: 5000 ms; FP: 0.5 MPa; FoT: 5000 ms; FoP: 1.0 MPa; HT: 7.5 s). The friction phase is most significant for the heat input, which is made evident by the effect of high values of rotational speed, friction time and friction pressure, which contribute to higher stake head temperatures.

### **Joint microstructure**

The microstructures of two F-ICJ joints that were produced using a 75° pin tool in two different processing conditions (low and high heat inputs) are shown in Figure 9. The stake head temperature measured for the low heat input

joint in Figure 9a was 47.4 °C, whereas for the high heat input joint from Figure 9b it was 74.2 °C.

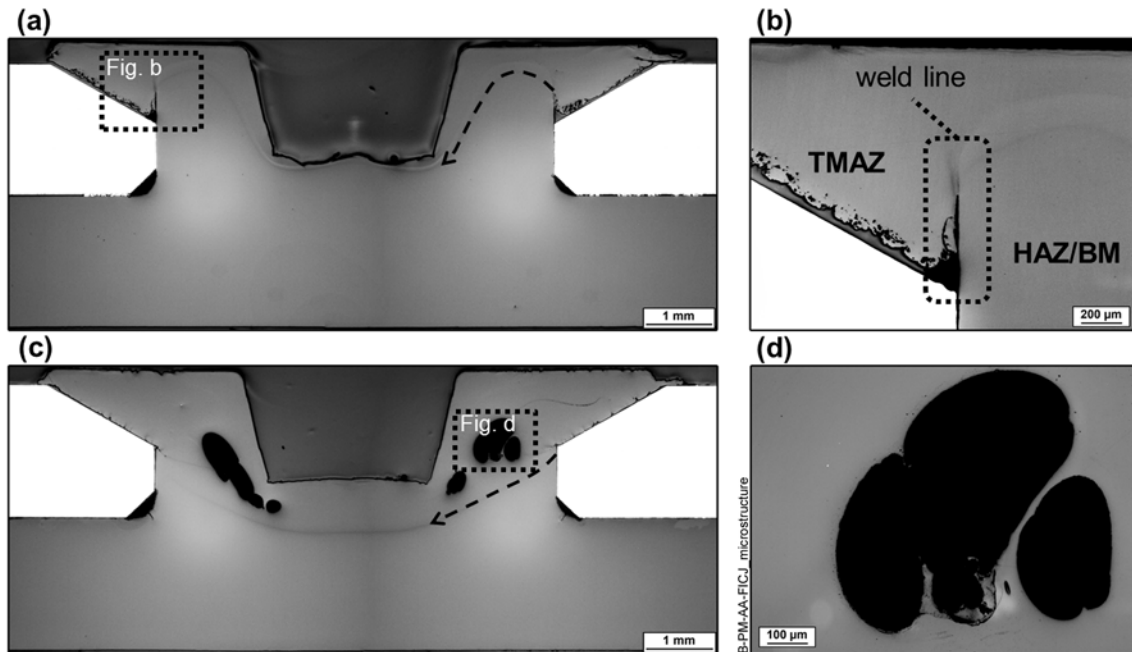


**Figure 9: Typical microstructures of F-ICJ joints that were produced using a 75° pin tool: (a) cross section of a low-heat-input joint (RS: 8000 rpm; FT: 2500 ms; FP: 0.3 MPa; FoT: 5000 ms; FoP: 0.7 MPa; HT: 7.5 s); (b) weld line highlighted in (a); (c) cross section of a high-heat-input joint (RS: 12000 rpm; FT: 5000 ms; FP: 0.3 MPa; FoT: 5000 ms; FoP: 0.7 MPa; HT: 7.5 s); (d) volumetric flaws highlighted in (c). The dashed lines in (a) and (c) show the radial profile of a transition border between the zones with different refraction indices of PEI, which indicate the microstructural changes.**

The amount of thermal energy that is generated by friction between the rotating tool and the polymeric stud affects the shape and size of the microstructural zones and may result in different features in the polymeric partner. Low values of rotational speed, friction time and friction pressure produce low heat input, which affects a smaller volume of polymer. The low heat input joint from Figure 9a displays a thin process-affected volume in the polymer partner. The highlighted region is magnified in Figure 9b to show a weld line. Because of the low heat conductivity of the PEI, low-heat-input conditions can only soften thin layers that are closer to the tool; therefore, a large volume of the formed stake remains unaffected by the process. The weld line is a polymer-polymer interface between these unaffected solid volumes and the material that flowed sideways because of squeeze flow and solidified over the chamfer. Again, the low heat input does not allow the healing of this interface. This feature can act as a notch, which causes crack nucleation in this area under mechanical loading. The high-heat-input joint from Figure 9c showed a larger process-affected volume in the polymer partner without visible presence of weld lines. The higher heat input could soften thicker layers of the material, which filled the cavities when the tool moved forward. In high-heat-input joints, the formation of volumetric flaws (Figure 9d) can occur. These flaws can be entrapped air, which originated from the low viscosity of the material at notably high temperatures. Other possible causes are the evolution of structural water (Stokes, 2001), evolution of volatile products of thermal degradation (Katayama and Kawahito, 2008), and/or thermal stresses induced during processing (Ahmed et al., 2006). Further investigation is required to understand the flaw formation mechanisms.

Another factor that affects the shape and size of the process-affected volume is the shape of the tool. Figure 10 shows joints that were produced using pin tools with angles of 75° and 30° under the processing condition: RS: 15000 rpm; FT: 2500 ms; FP: 0.4 MPa; FoT: 2500 ms; FoP: 0.8 MPa; HT: 10 s.

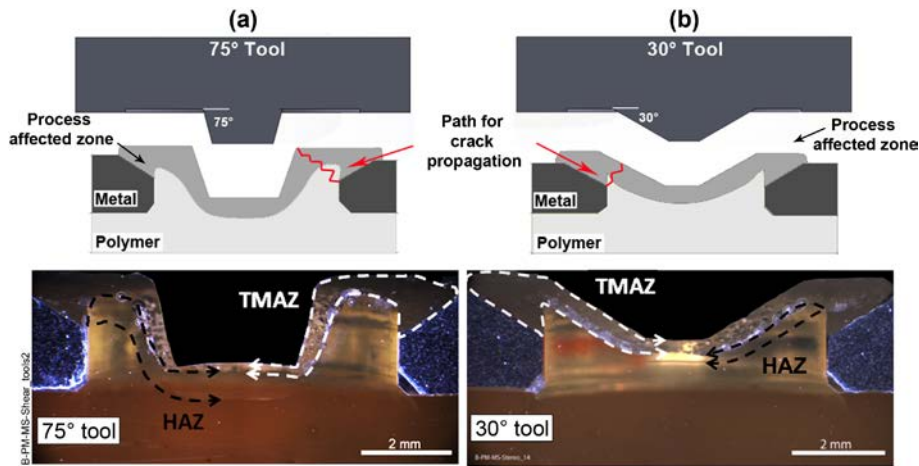


**Figure 10: Schematic drawings of the pin tools (75° and 30°), the produced joints and the stereomicroscopy macrographs of the joint cross-sections, which showed the influence of the pin tool angle on the shape and size of the microstructural zones and the crack propagation regime: (a) joint produced using a 75° pin tool; (b) joint produced using a 30° pin tool.**

Geometrically, the 75° pin tool produces a thicker wall for the hollow stake; therefore, it has a longer path for crack propagation in the stake than the joints that were produced using the 30° pin tool (Figure 10). The length of the crack propagation path can affect the global mechanical performance of the joint. A detailed description of the fracture mechanisms in F-ICJ is out of the scope of this manuscript and will be published in a separate document.

The 75° pin tool has a large pin radius and penetrates deeply into the polymeric stud. The 30° tool has a smaller pin radius and a shallow profile. Because of these differences, the tool geometry defines a unique shear profile in the polymeric stud, which can affect a larger or smaller volume of polymer depending on the processing conditions.

The effect of the pin tool geometry on the shear profiles that dictate the shape of the microstructural zones can be related to rheology theories using the analogies of polymer flow patterns, which are generated by each tool design with the drag shear flow profiles in cone-plate rheometers. The generated shear rate ( $\dot{\gamma}$ ) is proportional to the rotational speed ( $\Omega$ ) and inversely proportional to the cone angle ( $\Theta_0$ ) as described in Equation 1 (Dealy and Wissbrun, 1995). For F-ICJ,  $\Omega$  is the rotational speed of the tool, and  $\Theta_0$  is the tool angle.

$$\dot{\gamma} = \Omega / \Theta_0 \text{ [s}^{-1}\text{]} \quad (1)$$

Although Equation 1 relies on the assumptions of steady relative movement between the cone and the plate and small cone angles ( $2^\circ < \Theta_0 < 10^\circ$ ) (Dealy and Wissbrun, 1995), it can help to elucidate the shear layer development in F-ICJ joints. The use of a pin tool induces a profile in which the increase in radius (from the center to the edge) is balanced by an increase in height of the sheared volume. In cone-plate rheometry, this concept generates a uniform shear profile over the volume because of the small cone angles. In F-ICJ, the shear profile is not uniform as can be noticed in Figure 10 from the size and shape of the process-affected volumes. The 75° pin tool (Figure 10a) produces a thinner TMAZ around the keyhole than the 30° pin tool (Figure 10b), which is consistent with Equation 1: a smaller angle corresponds to a larger

induced shear rate. Thus, in F-ICJ, smaller pin angles create a thicker shear layer around the pin. In principle, a thick shear layer profile affects a larger volume of material and changes the material properties. Depending on the resulting local properties, this change might be undesirable. However, the larger shear layer helps pushing the material inside the cavities and achieving better mechanical anchoring. Therefore, the tool geometry should be designed according to the joint specifications and process optimization for improved cavity filling. Further studies are currently under progress to determine the influence of tool geometry on cavity filling.

### **Local mechanical properties**

Thermomechanical effects on the polymeric material can locally modify its mechanical properties. Figure 11 shows a microhardness distribution map (left-hand side) with the micrograph (right-hand side) of an F-ICJ joint that was produced using a 75° pin tool under the following processing condition: RS: 8000 rpm; FT: 5000 ms; FP: 0.3 MPa; FoT: 2500 ms; FoP: 0.7 MPa; HT: 7.5 s. The stake head temperature measured for this joint was 67.2 °C.

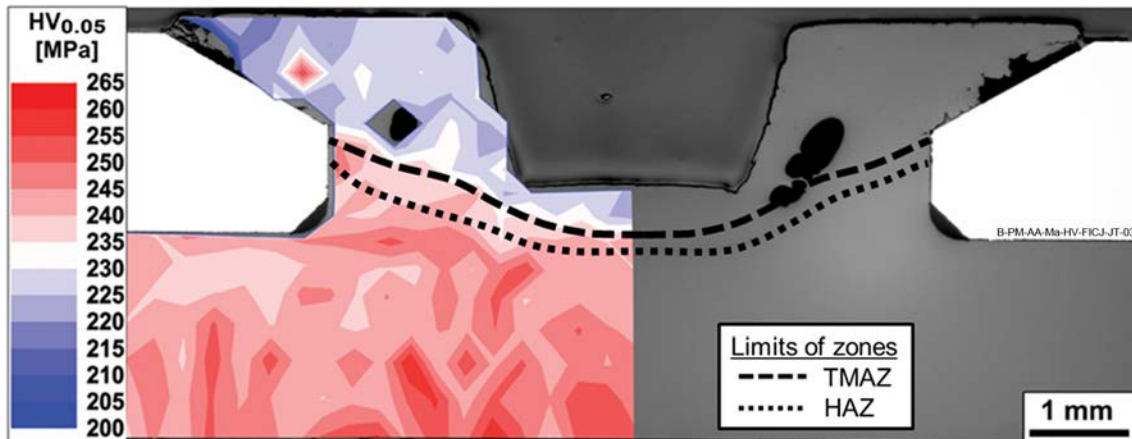


**Figure 11: Juxtaposition of the microhardness distribution map and micrograph for a typical F-ICJ joint that was produced using a 75° pin tool (RS: 8000 rpm; FT: 5000 ms; FP: 0.3 MPa; FoT: 2500 ms; FoP: 0.7 MPa; HT: 7.5 s). The microhardness measurements were performed on the displayed half of the cross section.**

The microhardness analysis helps to identify the microstructural zones created in the process. For the joint in Figure 11, three different zones could be defined in the polymer partner, which correspond to the TMAZ, HAZ and BM zones. The smallest microhardness values are observed at the thermomechanically affected zone (TMAZ,  $226 \pm 6$  MPa), which is the region that was most affected by the process. A thin zone adjacent to the TMAZ with intermediate microhardness values was identified as the heat affected zone (HAZ,  $236 \pm 5$  MPa). Under the HAZ is an unaffected volume with base material properties (BM,  $245 \pm 5$  MPa). The decrease in microhardness in the process-affected volumes compared to the base material may be associated to some physical chemical effects such as reorientation of chains and degradation by chain scission. These effects occur because of the thermomechanical treatment

and different cooling rates that were imposed by the process. This result was observed in similar friction-based processes such as FricRiveting (Amancio-Filho et al., 2008) and ultrasonic welding (Ghosh and Reddy, 2009). Low levels of degradation were shown by Amancio (2007) and Oliveira (2012) not to deteriorate the global mechanical performance of the joints, but excessive degradation can significantly affect the microstructure (Ghorbel et al., 2009) and the joint strength (Ghosh and Reddy, 2009). Table 1 shows the decrease in microhardness at the process-affected regions of the joint from Figure 11, which is compared to the base material properties that were obtained from measurements in a PEI stud prior to joining.

**Table 1: Example of change in local mechanical properties in an F-ICJ joint (75° pin tool; RS: 8000 rpm; FT: 5000 ms; FP: 0.3 MPa; FoT: 2500 ms; FoP: 0.7 MPa; HT: 7.5 s).**

<b>Measurement region</b>	<b>Average microhardness [MPa]</b>	<b>HV<sub>zone</sub> / HV<sub>PEI</sub></b>
PEI stud (base material)	246 ± 7	–
Base material at joined sample	245 ± 5	1.00
HAZ at joined sample	236 ± 5	0.96
TMAZ at joined sample	226 ± 6	0.92

Lower microhardness values in amorphous polymers represent the reduced chain packing density because of alterations at the molecular scale such as chain rotation/reorientation (Flores et al., 2009) or reduction in molecular weight (Rueda et al., 1981) as a result of partial degradation. Therefore, the microstructural changes over the stake volume can affect the global mechanical behavior; for example, regions with sharper morphology change can affect the crack growth path for the joined parts.

### **Global mechanical properties**

F-ICJ joints were subjected to single lap shear strength testing. In the studied processing window, the sound F-ICJ joints achieved ultimate lap shear load values that ranged from  $712 \pm 34$  N ( $30^\circ$  pin tool; RS: 20000 rpm; FT: 2500 ms; FP: 0.4 MPa; FoT: 2500 ms; FoP: 0.8 MPa; HT: 10 s) to  $1250 \pm 98$  N ( $75^\circ$  pin tool; RS: 12000 rpm; FT: 2500 ms; FP: 0.3 MPa; FoT: 5000 ms; FoP: 1.0 MPa; HT: 7.5 s). A typical load-displacement curve for an F-ICJ joint and its strain distribution, which are obtained from the DIC measurements during lap shear testing, are shown in Figure 12.

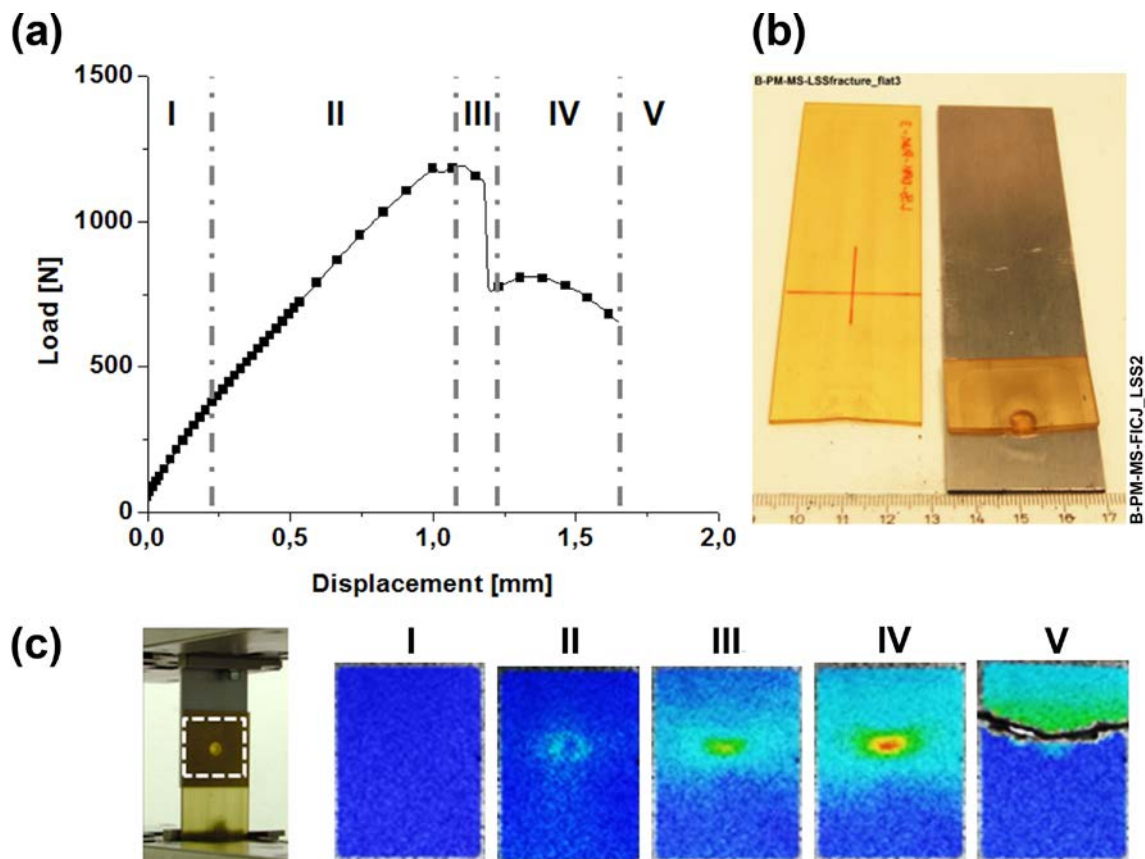


**Figure 12: Single lap shear testing of a F-ICJ joint: (a) typical load-displacement curve; (b) image of net tension failure mode; (c) strain distribution at the specimen surface through the test (75° pin tool; RS: 8000 rpm; FT: 5000 ms; FP: 0.3 MPa; FoT: 5000 ms; FoP: 1.0 MPa; HT: 7.5 s).**

The load-displacement curve first shows an elastic behavior (stage I). As the displacement increases, the stud rotation due to secondary bending is prevented by the stake head, and the strain is concentrated around the stake base (stage II). During stage II, a radial crack nucleates and propagates around the stake head. The loss of the stake head corresponds to the decrease in load in stage III. At this point, the load is no longer sustained by the head but by the

bearing of the stake on the internal cavities of the joining partner; the strain, which was initially concentrated around the stake base, is now redistributed along the width of the polymeric plate (stage IV). The strain and the load increase when the crack propagates in the base plate; finally, the plate fails by net-tension (stage V), as displayed in Figure 12b. This behavior is currently the most commonly observed behavior for sound F-ICJ joints.

Other less frequent failure modes are stake pull-out and head pull-out, both of which can occur depending on the stake head geometry and the variation in microstructural properties of the joints (Abibe et al., 2013). Figure 13 shows a schematic drawings of stake pull-out (Figure 13a) and head pull-out (Figure 13b) failure modes, and a macrograph of the longitudinal cross-section of the joints with these failure modes. Stake pull-out (sometimes referred to as “rivet pull-out”) is characterized by an incomplete crack in the base plate, which is notably similar to the net tension typical crack, although it is not catastrophic. Head pull-out also exhibits an identical incomplete crack; however, the joint failure is because of the loss of the stake head.

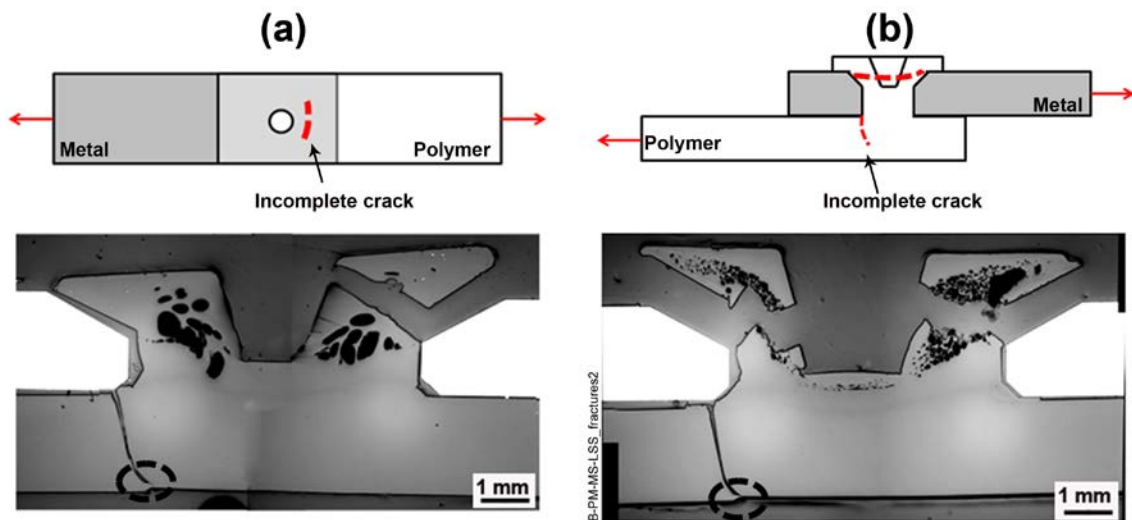


**Figure 13: Schematic drawings and macrograph of failure modes in lap shear strength testing: (a) stake pull-out (or “rivet pull-out”) and (b) head pull-out. There is no catastrophic failure in the base plate, as highlighted in the macrographs.**

Cross tensile tests were performed to evaluate the mechanical strength of the stake head. After the specimen was fixed, the polymer plate was pulled, and the metal plate remained stationary. Over the investigated parameters, the cross tensile strength values ranged from  $311 \pm 20$  N (75° pin tool; RS: 12000 rpm; FT: 5000 ms; FP: 0.3 MPa; FoT: 5000 ms; FoP: 0.7 MPa; HT: 7.5 s) to  $585 \pm 10$  N (75° pin tool; RS: 8000 rpm; FT: 2500 ms; FP: 0.5 MPa; FoT: 5000 ms; FoP: 1.0 MPa; HT: 7.5 s). Figure 14a shows a typical load-displacement curve, which was obtained from cross-tensile testing for a sound F-ICJ joint.

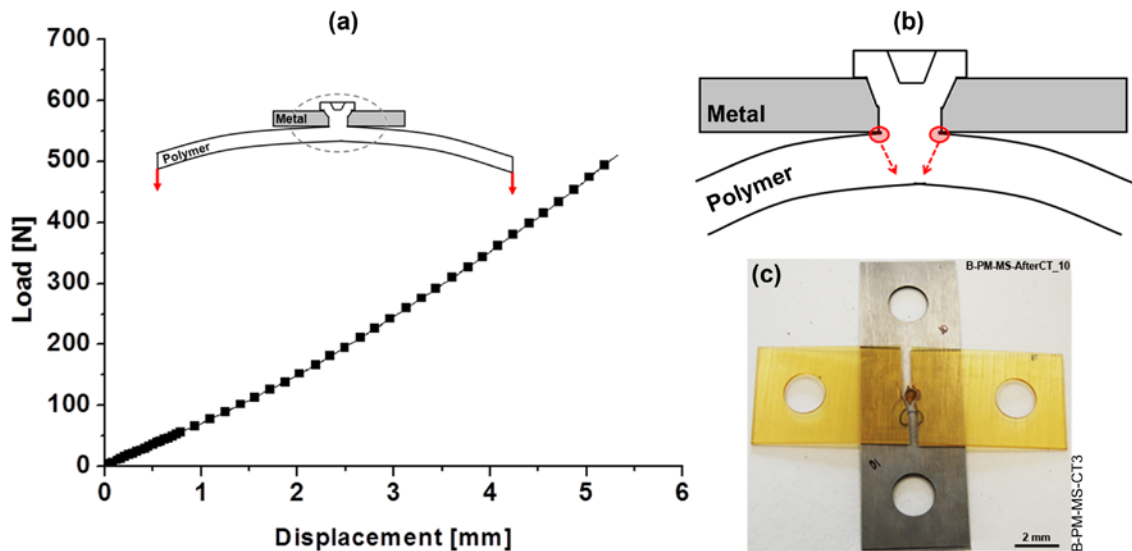


**Figure 14: Cross tensile testing and the observed failure mechanism for sound F-ICJ joints: (a) typical load-displacement curve and bending behavior from a specimen during cross tensile testing (75° pin tool; RS: 8000 rpm; FT: 2500 ms; FP: 0.5 MPa; FoT: 5000 ms; FoP: 1.0 MPa; HT: 7.5 s); (b) schematic drawing which shows the crack nucleation around the stake base and the crack propagation through the plate thickness; (c) surface view of the lower plate bending failure mode.**

A linear behavior is observed in the curve of Figure 14a when the polymer plate bends during the test until failure. This result indicates that a brittle fracture without yielding occurs (ASTM, 2010a). The bending causes nucleation and fast propagation of cracks in the stake base region through the plate thickness (Figure 14b), which leads to lower plate bending failure (Figure 14c). Failure by lower plate bending is the most frequently observed failure mode for sound F-ICJ joints in cross tensile testing.

Two other failure mechanisms of stake pull-out and head pull-out are observed in cross tensile testing although less frequently. These failure modes are currently not well understood. Figure 15 shows schematic drawings of these failure modes and macrographs of the cross-section of the joints that exhibit these mechanisms.

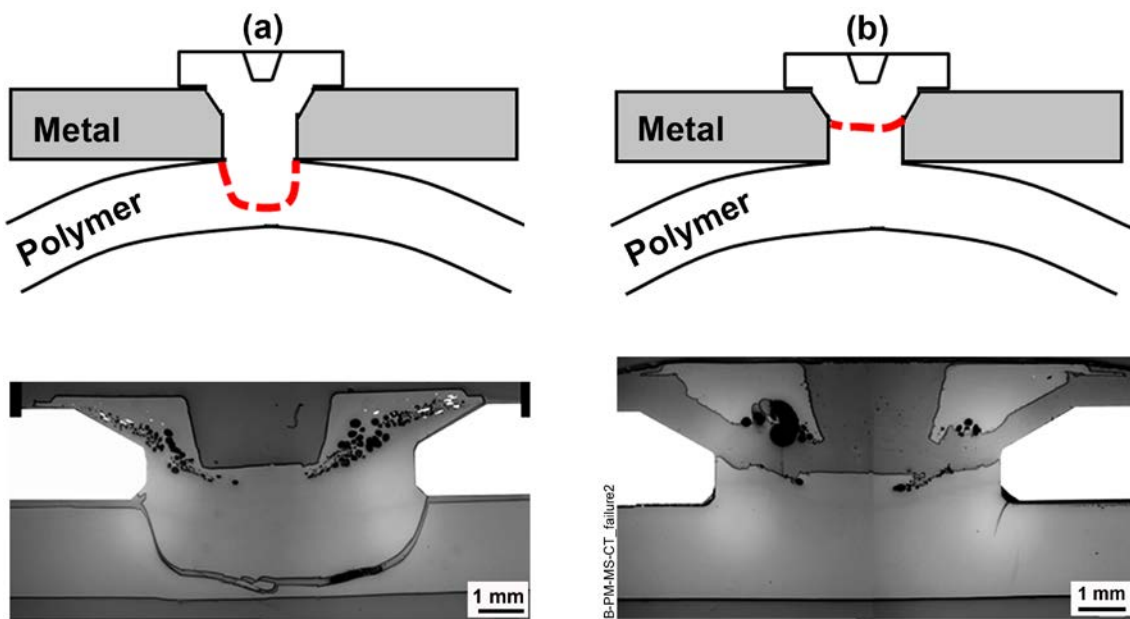


**Figure 15: Other failure modes that are observed in cross tensile test: (a) stake pull-out with crack propagation below the stake base and (b) head pull-out.**

Stake pull-out is a complete removal of the stake and its base from the polymer plate without complete cracking of the plate. The crack appears to nucleate around the stake base and propagate radially towards the center of the stake base, which detaches it from the base plate without damaging the stake head (Figure 15a). Head pull-out is shown in Figure 15b. In this case, the

premature failure is most likely because of defective stake heads with excessive amount of volumetric flaws or sharp weld lines.

## CONCLUDING REMARKS

This paper presented the primary features of the new Friction-based Injection Clinching Joining technique (F-ICJ) and demonstrated its feasibility for hybrid joints on material combinations of polyetherimide (PEI) and 6082-T6 aluminum alloy. The process phases, joining mechanisms, and general principles of the F-ICJ technology were explained. The relations of the process with the generated microstructure, and its effects on the mechanical performance of the joints were discussed.

The measured stake temperature after joining ranged from  $43 \pm 4$  °C to  $95 \pm 9$  °C. The achieved temperatures during a typical F-ICJ process are not sufficiently high to cause significant microstructural changes in the metal partner; however, three different microstructural zones were identified in the polymer partner: a thermomechanically affected zone (TMAZ), a heat affected zone (HAZ) and an unaffected volume with base material properties (BM). The heat input from the joining process affected the shape and size of the microstructural zones and may create weld lines and/or volumetric flaws. Moreover, the shape of the tool modifies the joint macrostructure and consequently the shape of the microstructural zones by changing the shear profile, which was produced during the tool rotation. Smaller pin tool angles create thicker shear layers (Figure 10). Therefore, the tool design should

consider the cavity profiles and joining partner's geometry to optimize the cavity filling without significantly changing the material properties. Differences in the local mechanical properties at the process-affected volumes were identified using microhardness testing with 4% decrease in the HAZ and 8% decrease in the TMAZ.

The global mechanical performance of the joints was evaluated using single lap shear tests. In this feasibility study, the maximum lap shear load values ranged from  $712 \pm 34$  N to  $1250 \pm 98$  N. The net tension is the most common failure mode, but variations can occur depending on premature stake head failure and microstructural features.

Cross tensile testing was used to measure the strength of the stake head. In these experiments, the maximum cross tensile load values ranged from  $311 \pm 20$  N to  $585 \pm 10$  N. For most specimens, the failure occurred by lower plate bending, which showed the high strength of the stake that was formed in F-ICJ. Specimens with defective stake heads may fail by head pull-out.

Failure in both lap shear and cross tensile testing does not appear largely influenced by the microstructural changes that are induced in the polymeric partner. The effect of the weaker TMAZ and HAZ regions is smaller than the notch effect from the weld lines and the increased stresses from secondary bending. Further investigation on the failure modes in lap shear and cross tensile tests must be performed.

Friction-based Injection Clinching Joining technique (F-ICJ) has been shown to be a promising joining technology for polymer-metal hybrid structures.

Compared to E-ICJ and current staking, F-ICJ has short cycles, high energy efficiency, while improving key joint characteristics such as aesthetics and mechanical performance.

## ACKNOWLEDGEMENTS

The authors acknowledge the financial support that was provided for the Young Investigator Group “Advanced Polymer-Metal Hybrid Structures” by the Helmholtz Association Germany.

## REFERENCES

- Aalco, 2011. Aluminium Alloy 6082 - T6~T651. Aalco Metals.
- Abibe, A.B., Amancio-Filho, S.T., Dos Santos, J.F., Hage, E., 2011. Development and Analysis of a New Joining Method for Polymer-Metal Hybrid Structures. *J. Thermoplast. Compos. Mater.* 24, 233-249. [10.1177/0892705710381469](https://doi.org/10.1177/0892705710381469).
- Abibe, A.B., Amancio-Filho, S.T., dos Santos, J.F., Hage, E., 2013. Mechanical and failure behaviour of hybrid polymer-metal staked joints. *Materials and Design* 46, 338-347.
- Adderley, C.S., 1988. Adhesive Bonding. *Materials & Design* 9, 287-293. [http://dx.doi.org/10.1016/0261-3069\(88\)90006-4](http://dx.doi.org/10.1016/0261-3069(88)90006-4).
- Ahmed, T.J., Stavrov, D., Bersee, H.E.N., Beukers, A., 2006. Induction welding of thermoplastic composites—an overview. *Composites Part A: Applied Science and Manufacturing* 37, 1638-1651. <http://dx.doi.org/10.1016/j.compositesa.2005.10.009>.
- Amancio-Filho, S.T., Dos Santos, J.F., Beyer, M., 2010. Method and device for connecting a plastic workpiece to a further workpiece, US 7,780,432 B2, USA.
- Amancio-Filho, S.T., Roeder, J., Nunes, S.P., dos Santos, J.F., Beckmann, F., 2008. Thermal degradation of polyetherimide joined by friction riveting (FricRiveting). Part I: Influence of rotation speed. *Polymer Degradation and Stability* 93, 1529-1538. <http://dx.doi.org/10.1016/j.polymdegradstab.2008.05.019>.
- Amancio, S., 2007. Friction Riveting: development and analysis of a new joining technique for polymer-metal multi-materials structures. Technische Universität Hamburg-Harburg, Ph.D. Dissertation

Amancio, S.T., dos Santos, J.F., 2009. Joining of Polymers and Polymer-Metal Hybrid Structures: Recent Developments and Trends. *Polymer Engineering and Science* 49, 1461-1476. [10.1002/pen.21424](https://doi.org/10.1002/pen.21424).

ASTM, 2010a. D790-10.

ASTM, 2010b. D5961-10.

ASTM, 2010c. E384-10e1.

Barnes, T.A., Pashby, I.R., 2000. Joining techniques for aluminium spaceframes used in automobiles: Part II — adhesive bonding and mechanical fasteners. *Journal of Materials Processing Technology* 99, 72-79. [http://dx.doi.org/10.1016/S0924-0136\(99\)00361-1](http://dx.doi.org/10.1016/S0924-0136(99)00361-1).

Beute, S., 2009. Infrastake - Staking At The Speed Of Light, SPE ANTEC 2009. Curran Associates, Inc., Chicago, USA, pp. 1723-1727.

Billmeyer Jr, F.W., 1971. *Textbook of polymer science*, 2 ed. Wiley-Interscience, New York.

Carrocio, S., Puglisi, C., Montaudo, G., 2012. Polyetherimide, In: Thomas, S., Visakh, P.M. (Eds.), *Handbook of Engineering and Specialty Thermoplastics*. Scrivener Publishing LLC, Salem, MT, pp. 79-110.

Chao, Y.J., Qi, X., Tang, W., 2003. Heat Transfer in Friction Stir Welding—Experimental and Numerical Studies. *Journal of Manufacturing Science and Engineering* 125, 138-145. <http://dx.doi.org/10.1115/1.1537741>.

Chen, Q., Li, D.Y., 2005. A computational study of frictional heating and energy conversion during sliding processes. *Wear* 259, 1382-1391. <http://dx.doi.org/10.1016/j.wear.2004.12.025>.

Cuenot, F., 2009. CO2 emissions from new cars and vehicle weight in Europe; How the EU regulation could have been avoided and how to reach it? *Energy Policy* 37, 3832-3842. <http://dx.doi.org/10.1016/j.enpol.2009.07.036>.

Dealy, J.M., Wissbrun, K.F., 1995. Rotational and Sliding Surface Rheometers, In: Dealy, J.M., Wissbrun, K.F. (Eds.), *Melt Rheology and Its Role in Plastics Processing: Theory and Applications*. Chapman & Hall, London, pp. 269-297.

DeSouza, R., 2009. Characterization and Guideline Development of the Heat Staking Process. University of Toronto, Bachelor Thesis

DIN, 2002. DIN EN ISO 14272.

Duflou, J.R., De Moor, J., Verpoest, I., Dewulf, W., 2009. Environmental impact analysis of composite use in car manufacturing. *CIRP Annals - Manufacturing Technology* 58, 9-12. <http://dx.doi.org/10.1016/j.cirp.2009.03.077>.

Flores, A., Ania, F., Baltá-Calleja, F.J., 2009. From the glassy state to ordered polymer structures: A microhardness study. *Polymer* 50, 729-746. <http://dx.doi.org/10.1016/j.polymer.2008.11.037>.

Ghorbel, E., Casalino, G., Abed, S., 2009. Laser diode transmission welding of polypropylene: Geometrical and microstructure characterisation of weld. *Materials & Design* 30, 2745-2751. <http://dx.doi.org/10.1016/j.matdes.2008.10.027>.

Ghosh, S., Reddy, R., 2009. Ultrasonic sealing of polyester and spectra fabrics using thermo plastic properties. *Journal of Applied Polymer Science* 113, 1082-1089. <http://dx.doi.org/10.1002/app.30050>.

Hahn, O., Finkeldey, C., 2003. Ultrasonic Riveting and Hot-Air-Sticking of Fiber-Reinforced Thermoplastics. *J. Thermoplast. Compos. Mater.* 16, 521-528. <http://dx.doi.org/10.1177/089270503032852>.

Katayama, S., Kawahito, Y., 2008. Laser direct joining of metal and plastic. *Scripta Materialia* 59, 1247-1250. <http://dx.doi.org/10.1016/j.scriptamat.2008.08.026>.

Messler Jr, R.W., 1995. The challenges for joining to keep pace with advancing materials and designs. *Materials & Design* 16, 261-269. [http://dx.doi.org/10.1016/0261-3069\(96\)00004-0](http://dx.doi.org/10.1016/0261-3069(96)00004-0).

Neumann, A., Schober, D., 1991. *Reibschweißen von Metallen*. Verlag Technik GmbH, Berlin, Germany.

Oliveira, P.H.F., 2012. Estudo das propriedades e desempenho mecânico de juntas soldadas por fricção pontual de poli (metacrilato de metila) (PMMA). UFSCar, Master Thesis

- Potente, H., 2004. Schweißen, In: Potente, H. (Ed.), Fügen von Kunststoffen: Grundlagen, Verfahren, Anwendung. Carl Hanser Verlag, Munich, pp. 109-259.
- Rotheiser, J., 1999. Joining of Plastics: Handbook for Designers and Engineers. Carl Hanser Verlag, Munich.
- Rueda, D.R., Baltá Calleja, F.J., Bayer, R.K., 1981. Influence of processing conditions on the structure and surface microhardness of injection-moulded polyethylene. *J Mater Sci* 16, 3371-3380. <http://dx.doi.org/10.1007/BF00586299>.
- Schaefer, R., 1971. Beitrag zum Reibschweißen von Metallen unter besonderer Berücksichtigung der Energieumwandlung während des Schweißprozesses. Rheinisch-Westfälische Technische Hochschule Aachen, Aachen, Ph.D. Dissertation
- Stokes, V.K., 1988a. Analysis of the friction (spin)-welding process for thermoplastics. *J Mater Sci* 23, 2772-2785. <http://dx.doi.org/10.1007/BF00547450>.
- Stokes, V.K., 1988b. Vibration welding of thermoplastics. Part II: Analysis of the welding process. *Polymer Engineering & Science* 28, 728-739. <http://dx.doi.org/10.1002/pen.760281105>.
- Stokes, V.K., 2001. A phenomenological study of the hot-tool welding of thermoplastics Part 3. Polyetherimide. *Polymer* 42, 775-792. [http://dx.doi.org/10.1016/S0032-3861\(00\)00395-5](http://dx.doi.org/10.1016/S0032-3861(00)00395-5).
- Yeh, H.J., Schott, C.L., Park, J.B., 1998. Experimental study on hot-air cold staking of PC, PC/ABS and acetal samples, SPE ANTEC 1998. Society of Plastics Engineers, Atlanta, USA, pp. 1078-1083.